Aging of an Al-Mg-Si Alloy with a Silicon Excess and Reinforced with Ceramic Particles

G. MEYRUEY, V. MASSARDIER, and M. PEREZ

The aging of an Al-Mg-Si alloy with a high silicon excess and reinforced with ceramic particles was characterized between 373 K and 623 K to understand how the particles affect: (i) the precipitation kinetics of coherent and semi-coherent phases, (ii) the precipitation sequence of the alloy, and (iii) the loss of mechanical strength from a peak-aged microstructure obtained by a T6 treatment. Compared with the unreinforced alloy, heterogeneous precipitation of disordered semi-coherent phases occurs on dislocations and the precipitation kinetics were found to be accelerated in the composite leading to an acceleration of the loss of strength from the T6 condition, due to the precipitation of the Type-C phase. An experimental isothermal transformation curve was proposed for the composite and compared with that of the unreinforced alloy. Then, a study was performed on a deformed alloy to demonstrate that most of the differences observed between the unreinforced alloy and the composite can be explained by the high dislocation density generated in the matrix of the composite due to the presence of ceramic particles. Lastly, the decrease in mechanical strength occurring during isothermal treatments from the T6 state could be successfully modeled using the JMAK approach.

https://doi.org/10.1007/s11661-020-05736-x

I. INTRODUCTION

IN a recent paper,[1] the overaging of an Al-Mg-Si alloy with a high silicon excess was investigated by combining both global and local techniques. This type of alloy is particularly interesting from an industrial point of view with respect to pseudo-binary age-hard-enable Al-Mg_2Si alloys. Indeed, numerous studies have reported that the presence of a silicon excess tends to increase the maximum mechanical strength reached by the alloy during a T6 treatment (typically 8 hours at 443 K (170 °C) and highlighted that the greater the silicon excess, the greater the mechanical strength.[2,3] However, there are two main drawbacks associated with silicon excess: (i) the acceleration of the overaging phenomena leading to a sharp drop in mechanical strength after having reached the peak strength and (ii) a complexification of the precipitation sequence. This is particularly notable in the temperature domain of the semi-coherent precipitation where the β' phase (HCP, $a = 0.705$ nm, $c = 0.405$ nm) typical of the quasi-binary alloys and its precursor, denoted here β'_0, (HCP, $a = 0.407$ nm, $c = 0.405$ nm), can be replaced or coexist with phases specific to Al-Mg-Si alloys with silicon excess such as the phases of Type-A (HCP, $a = 0.705$ nm, $c = 0.67$ nm), Type-B (orthorhombic, $a = 0.68$ nm, $b = 0.79$ nm, $c = 0.405$ nm), and Type-C (HCP, $a = 1.04$ nm and $c = 0.405$ nm).[4–12]

In the study presented in paper,[1] the precipitation kinetics of the investigated alloy (initially homogenized and water-quenched) were first followed indirectly by ThermoElectric Power (TEP) and Vickers hardness measurements during isothermal treatments performed at temperatures between 373 K and 623 K (100 °C and 350 °C). The complex TEP variations detected during aging were found to be perfectly correlated with the hardness variations, indicating that TEP is sensitive to overaging. Secondly, the treatment conditions leading to important TEP and hardness variations were characterized by Conventional and High-Resolution Transmission Electron Microscopy (C-TEM and HR-TEM) and by Atom Probe Tomography (APT). This led us to define the following precipitation sequence between 373 K and 573 K (100 °C and 300 °C)[1]:

$$\beta'' \rightarrow \beta'' + \text{Type - B} \rightarrow \text{Type - B/Type - A/Type - C} \,/\beta' + \text{Si particles} \rightarrow \text{Type - A} + \text{Type - C} + \text{Si particles}.$$

The precipitation of the β'' phase occurs in the early stages of aging. It was found to be responsible for the increase in strength of the alloy to its maximum value

G. MEYRUEY, V. MASSARDIER, and M. PEREZ are with the University of Lyon, INSA Lyon, MATEIS – UMR CNRS 5510, Bât. Saint-Exupéry, 25 Avenue J. Capelle, 69621 Villeurbanne Cedex, France. Contact email: veronique.massardier@insa-lyon.fr
Manuscript submitted September 24, 2019.

Published online: 09 April 2020

and for the sharp TEP decrease to a minimum value detected on the TEP kinetics. Then, with further aging, it was observed that hardness decreases while TEP increases at the same time. This was attributed to the precipitation of the semi-coherent Type-B phase, followed by the precipitation of the Type-A and Type-C semi-coherent phases. From the correlation between the evolution in TEP and the microstructural changes occurring in the alloy, a part of the isothermal transformation curve of the alloy could be built between 373 K and 623 K (100 °C and 350 °C).

Thirdly, starting from a T6 state, the alloy's loss of mechanical strength during isothermal aging was followed between 373 K and 623 K (100 °C and 350 °C) by hardness measurements and it was successfully modeled using a simple empirical approach based on the Johnson–Mehl–Avrami–Kolmogorov (JMAK) formalism.

For specific applications in aerospace, aeronautic and automotive fields[13–15] requiring a combination between lightweight, high mechanical properties at elevated temperatures and good conductivity properties, ceramic particles (such as silicon or boron carbides) can be added to an aluminum matrix such as the one investigated in paper.[1] The ceramic particles provide a higher wear resistance to the alloy and enable to maintain good strength properties when the temperature is increased. The presence of these particles is expected to have a strong influence on the aging and overaging of the alloy due to the microstructural modifications induced by the particles: (i) decrease in the grain size,[16] (ii) presence of numerous interfaces, (iii) increase in the dislocation density generated during the cooling from the solutionizing temperature as the thermal expansion coefficients of the matrix and reinforcement are very different,[17–19] and (iv) residual stresses.[20,21] In the above mentioned context, the aim of the present study is to understand how the ceramic particles act on the alloy's behavior taking into consideration: (i) precipitation kinetics, (ii) microstructural evolution, and (iii) mechanical strength modifications during aging and more particularly, from the T6 state.

In the literature, several studies aimed at analyzing the effects of the reinforcing particles on the precipitation kinetics of the different phases have been carried out. It has been proved that these effects depend on several parameters: volume fraction, morphology, size and nature of the reinforcement,[16,22–24] nature of the alloying elements in the matrix,[25] type of precipitates and the fabrication technique of the material. Table I gives a brief review of some results which were reported in literature on this subject, where the aluminum matrix is an Al-Mg-Si alloy without silicon excess (notably, a 6061 alloy which has been the subject of many studies).

Concerning the GP zone formation, no clear conclusion can be drawn from the results found in the literature, as some authors have suggested that this metallurgical phenomenon could be unaffected by the reinforcement,[26–28] or accelerated,[26,29] or delayed[28,30,31] due to a possible entrapment of the quenched-in vacancies by the sinks present in the matrix

Table I. Effect of the Presence of Ceramic Reinforcement in a 6061 Alloy on the Precipitation Kinetics of the GP Zones and of the β″ and β′ Phases

Phase	Materials	Fabrication Technique	Characterization Technique	Effect of Reinforcement	References
GP zones	6061 + 10/20 vol. pct SiC	powder metallurgy	TEP	acceleration during natural aging but no effect during aging at 348 K (75 °C)	26
	6061 + 17.5 vol. pct SiCw	squeeze-casting	brinell hardness	slower precipitation	28
	6061 + 13.9 vol. pct SiCp	powder metallurgy	DSC	no effect	
	6061 + 20 vol. pct SiCw	powder metallurgy	DSC	suppression	30
β″	6061 + 20 vol. pct SiCw	powder metallurgy	DSC	acceleration	30
	6061 + 10/20 vol. pct SiC	powder metallurgy	TEP	acceleration	26
	6061 + 23 vol. pct B_4C	powder metallurgy	brinell hardness	acceleration	34
β′	6061 + 10/20 vol. pct SiC	powder metallurgy	TEP	acceleration	26
	6061 + 21 vol. pct SiCw	squeeze-casting	DSC	acceleration	38

(dislocations or interfaces). They may even be suppressed.[30,32,33]

With regard to the precipitation of the β'' coherent phase, the results are in favor of an acceleration in the presence of ceramic particles. This effect was highlighted by different characterization techniques: hardness,[17,34–36] TEP[32] or Differential Scanning Calorimetry (DSC).[34] The main explanation is that the acceleration could be due to an enhanced diffusion of the alloying elements resulting from the presence of : (i) residual stresses,[36,37] (ii) interfaces,[34] and/or (iii) dislocations.[26,30]

Lastly, it has been frequently observed that the precipitation of the β' semi-coherent phase is accelerated in the reinforced alloys, using various experimental techniques (DSC,[38] hardness,[34–36] and TEP[39,40]). In this case, the increased dislocation density of the reinforced alloys is generally considered to be responsible for its effect, as the dislocations could provide preferential nucleation sites for heterogeneous precipitation.

In spite of all the studies on the effects of the addition of ceramic particles to Al-Mg-Si alloys, the prediction of the behavior of the reinforced matrix during aging remains difficult. This is particularly true in the case of the Al-Mg-Si alloys with silicon excess for which the effects of the presence of ceramic particles on the precipitation kinetics, the precipitation sequence, and the mechanical behavior during aging have not been analyzed in detail so far.

This is why the present paper aims to investigate all these aspects. For this purpose, we chose to work on the same alloy that was studied in paper[1] but it was reinforced with 10 pct of carbide particles to be able to directly compare the behavior of the reinforced and unreinforced alloy. From an experimental point of view, the same approach as was described in paper[1] was used to build the isothermal transformation curve of the reinforced alloy. This approach is based on the coupling of indirect techniques (TEP, hardness, DSC) to follow the precipitation kinetics and direct techniques (C-TEM and HR-TEM) to identify the precipitates responsible for the TEP and hardness variations. In addition, the loss of mechanical strength of the T6-treated reinforced alloy was followed during isothermal aging between 373 K and 623 K (100 °C and 350 °C) and analyzed with the Johnson–Mehl–Avrami–Kolmogorov (JMAK) formalism to highlight the effect of the reinforcement. Lastly, for a more specific analysis of the role of the increased dislocation density in the matrix of the composite on the changes observed between the alloy and the composite both from a microstructural and mechanical point of view, the effect of the addition of a high density of dislocations in the unreinforced alloy was discussed and compared to the effect of the ceramic particles in the same alloy.

II. MATERIAL AND EXPERIMENTAL PROCEDURE

A. *Material*

The metal matrix composite used in the present study is an Al-Mg-Si alloy reinforced with 10 pct of carbide particles. The chemical composition of the alloy used as a matrix is Al-0.9 wt pct Mg_2Si-0.7 wt pct Si with a content in Fe and Mn of between 0.1-0.3 wt pct and 0.5-0.7 wt pct, respectively. During the processing of the composite, the carbide particles were added to the molten metal. Great care was taken to minimize the risk of interfacial reaction between the matrix and the reinforcement.

The particles used as reinforcement have an irregular morphology as illustrated in Figure 1. Their size is between 15 and 20 μm and their thermal dilatation coefficient is of the order of $6 \times 10^{-6} K^{-1}$.

To study the complete precipitation sequence of the investigated Al-Mg-Si alloy in the presence of ceramic particles and to follow the precipitation kinetics during isothermal treatments, the samples were first solution treated for 1 hour at 813 K (540 °C) in a salt bath and water-quenched. Before being isothermally treated, the samples were stored at 193 K (− 80 °C) to prevent any potential aging at room temperature. Then, for the study, the samples were artificially aged at temperatures between 373 K and 623 K (100 °C and 350 °C). These treatments were interrupted, at different intervals, to perform ThermoElectric Power (TEP) and Vickers hardness measurements at room temperature. For specific aging conditions, a detailed characterization of the precipitation state was conducted by different techniques according to the procedure described in Section II–C.

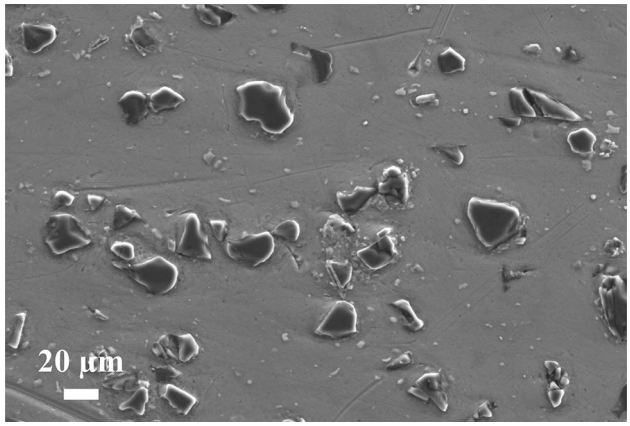

Fig. 1—SEM image showing the morphology of the carbide particles.

B. *Aging Kinetics*

To follow the microstructural and mechanical changes occurring during aging treatments in the unreinforced and reinforced alloy and to highlight the influence of the ceramic particles, ThermoElectric Power and hardness measurements were used, as in the case of paper.[1] These two techniques are briefly described below; more details were given in the previous study.[1]

1. *ThermoElectric power kinetics*

ThermoElectric Power measurements (TEP) were performed at room temperature on samples 70 mm long, 5 mm wide and 1 mm thick. The principle of the measurements is to apply a temperature difference (ΔT) at the two junctions between the studied sample and two blocks of pure aluminum and to measure the voltage (ΔV) created at the two junctions due to the Seebeck effect. The apparatus then gives the relative TEP of the sample with respect to that of pure aluminum defined by the following relation:

$$S = S_{\text{sample}} - S_{\text{pure aluminum}} = DV/DT. \qquad [1]$$

The standard error of the TEP measurements discussed in this work was estimated to $\pm$ 0.002 μV/K for the alloy and to $\pm$ 0.003 μV/K for the composite.

To follow the precipitation, the TEP of the materials investigated in this study was measured: (i) in the as-quenched state from the solutionizing temperature and (ii) in each state treated for a time t at temperature T so that the TEP variations noted $\Delta S_p(T,t)$ between these two states could be calculated for different treatment conditions. $\Delta S_p(T,t)$ is assumed to be the result of two major contributions: one due to the alloying elements in solid solution (ΔS_{ss}) and the other due to the precipitates themselves (ΔS_{pre}).

The effect of the alloying elements in solution on the diffusional component of the TEP of aluminum (ΔS_{ss}) is given, in the case of dilute alloys with several types of solute atoms, by the Gorther-Nordheim rule as defined previously.[1,41,42] In this relation, the contribution of each type of solute atom in solution depends on its specific resistivity (α_i), its specific TEP (S_i) and its weight concentration (C_i). Based on the values reported in the literature for the α_i and S_i coefficients[1,43] for the major alloying elements present in Al-Mg-Si alloys, it may be pointed out that magnesium and copper in solution in aluminum have a positive influence on the TEP value, while silicon has a negative influence lower than the positive influence of magnesium. This is why, if we do not take into account the effect of the precipitates, the simultaneous departure of the same amount of magnesium and silicon from the solid solution is expected to lead to a decrease in TEP.

With regard to the coherent or semi-coherent precipitates (GP zones, β'', β'...) created during the thermal aging of the alloy, they are likely to have an intrinsic effect on TEP which is known to depend on several parameters: size, shape, and volume fraction of precipitates.[44,45]

Previous studies[38] have shown that the small and coherent β'' phase has a strong negative influence on TEP, while the semi-coherent β' phase has a lower negative influence. It is for this reason that TEP strongly decreases during the β'' precipitation and reaches a minimum value at the end of this precipitation, before slightly increasing when β'' is gradually replaced by β'. Concerning the incoherent precipitates, such as the β-Mg_2Si phase, they are considered to have no influence on the TEP value.[46]

In the case where the TEP measurements are performed on an alloy reinforced with ceramic particles, it has been established[26] that the TEP variations are roughly equal (or proportional) to the TEP variations of the alloy used as matrix.

2. *Hardness kinetics*

To determine the evolution of the mechanical strength of the reinforced and unreinforced alloy under various aging conditions, Vickers hardness measurements were carried out on samples 5 mm thick with an applied load of 1 kg. Measurements were taken on a BUEHLER Micromet 5100 apparatus. For each aging treatment, 10 measurements were performed. The standard error of the hardness measurements performed in this study was estimated to be equal to $\pm$ 1 H_v for the alloy and to $\pm$ 3 H_v for the composite.

3. *Differential scanning calorimetry (DSC)*

DSC experiments were performed using a LABSYS EVO apparatus from SETARAM. The DSC samples were first homogenized with a treatment at 813 K (540 °C) and then cut to fill the crucible. The samples were heated from room temperature to 723 K (450 °C) at a constant heating rate of 10 K/min under an Argon atmosphere so that most of the alloying elements are precipitated in the form of stable coarse precipitates at the end of the first scan. The baseline was then determined by reheating specimens at the same heating rates and it was subtracted from the thermogram obtained during the first scan.

C. *Microstructural Characterization of the Precipitation States*

Transmission Electron Microscopy (TEM) was used for microstructural characterization to explain the mechanisms responsible for the main TEP and hardness variations observed during thermal treatments. After having selected appropriate aging states, it was then possible to establish the precipitation sequence of the studied alloy when it is used as a metal matrix for composite. Various information could be obtained about each type of precipitate, such as their size, crystallography, and morphology, enabling a comparison between the precipitates formed in the unreinforced alloy and in the composite.

For the preparation of the thin foils of the composite, the extracted foils were firstly, mechanically thinned from the bulk material already treated, and then thinned by an ion beam for a few hours (with 4 keV and an angle of 4 deg). In the case of the unreinforced alloy used for

comparison, the microstructural observations were performed on thin foils which were prepared according to a standard procedure (mechanical polishing, punching and double jet-polishing). A solution of 30 pct nitric acid and 70 pct of methyl alcohol was used at a temperature of 253 K (− 20 °C) and with a voltage of 20 V for electropolishing.

First, Conventional TEM (C-TEM) observations were performed on a Jeol 2100 microscope working at 200 kV and equipped with a CCD camera (Gatan Orius SC1000), leading to the determination of the precipitate dimensions and morphology. To identify the nature of the phases formed in the different states, High-Resolution TEM (HR-TEM) observations were carried out on a field-emission gun Jeol 2010 microscope with an accelerating voltage of 200 kV. The precipitates were observed along a $\langle 100 \rangle_{Al}$-zone axis; numerical Fast-Fourier Transforms (FFT) of the recorded images with the CCD camera were obtained and allowed us to differentiate the different types of precipitates.

D. *Determining the Dislocation Density by ECCI*

The dislocation density was estimated in this study to show the role of the dislocations in the matrix of the composite on precipitation and in the loss of mechanical strength. To achieve this, the electron channeling contrast imaging (ECCI) technique was applied to the composite. This technique, detailed in the literature,[47–49] can be used to identify crystal defects such as dislocations and is based on the quantity of back-scattered electrons after the interaction between the beam, when it penetrates the lattice, and nucleus.

Using a SEM in back-scattered electron mode, an acceleration voltage of 20 kV and selecting a grain in Bragg conditions on the thin foils prepared for TEM observations, the dislocations appear as white lines. As the dislocations generate contrast and can be differentiated from the grain, the dislocations can be counted. Then, the dislocation density can be estimated using the intercept method and the following equation[50,51]:

$$\rho = \frac{N}{L_r t}, \qquad [2]$$

where ρ is the dislocation density, N the number of intersections obtained with the intercept method, L_r the cumulative length of lines drawn and t the thickness interacting with the beam (estimated with the CASINO software[52]).

The ECCI technique was used in this work as an alternative method. This technique avoids the difficulties of observing dislocations by TEM near the ceramic particles, since carbide/matrix interfaces near the hole of the thin foils are most of the time not visible due to the sample preparation for TEM characterization. However, the results obtained by ECCI method are expected to be affected by the limited spatial resolution (10-20 nm)[53] of this technique. Besides, only one 2-beam condition is considered for the dislocation density estimation. As a result, some dislocations, which may be in extinction condition, can be not visible.[53] Considering the mentioned limitation, the density measurement may be slightly biased.

III. RESULTS

A. *Study of the Precipitation from a Supersaturated Solid Solution State*

1. *Isothermal precipitation kinetics of the reinforced and unreinforced alloy followed by hardness and TEP*

Figure 2 shows the hardness evolution of the unreinforced alloy and of the corresponding composite during isothermal aging treatments at 443 K and 523 K (170 °C and 250 °C) after quench from the solid solution state. This comparison highlights several differences due to the presence of the carbide particles in the alloy.

First, the initial hardness value is increased by the addition of ceramic particles. More than just the particles themselves, this difference can be justified by the higher dislocation density in the matrix of the composite after quench from the solid solution state coming from the difference in thermal expansion coefficient, between the aluminum matrix and the ceramic particles.

Then, in Figure 2, it can be noted that the hardness evolution can be divided in three distinct domains (*I*, *II*, *III*) for which the alloy and its composite present different responses.

Taking into account the results of paper,[1] the slight hardness increase detected in the first domain (*I*) at 443 K (170 °C) could be attributed to the GP zone precipitation, while the slight hardness decrease visible at 523 K (250 °C) results from the dissolution of the GP zones (which formed during the quench from the solutionizing temperature). At 443 K (170 °C), it may be noted that (i) the kinetics of GP zone formation is very similar for both materials and (ii) the magnitude of the hardness increase due to the GP zone formation is of the same order of magnitude for both materials, suggesting that the GP zone density is more or less the same in the composite and in the alloy and that the quenched-in vacancies necessary for the GP zone formation are not strongly affected by the sinks (interfaces, dislocations) present in the matrix of the composite. The tendencies are similar at 523 K (250 °C) for the phenomenon of GP zone dissolution.

In the second domain (II), hardness starts to increase significantly until reaching a maximum value, which can be attributed to the precipitation of the β'' coherent phase.[1] The hardness increment due to this precipitation is of the same order of magnitude in the unreinforced alloy and in the composite and is less pronounced at 523 K (250 °C) than at 443 K (170 °C) (T6 state) as the microstructure is expected to be finer and denser in the T6 state. However, one can note that the composite reaches its maximum value (after 4 hours at 443 K (170 °C) or 8 minutes at 523 K (250 °C)) before that of the unreinforced alloy, reached after 8 hours at 443 K (170 °C) or 15 minutes at 523 K (250 °C). This is consistent with the acceleration of the β'' precipitation

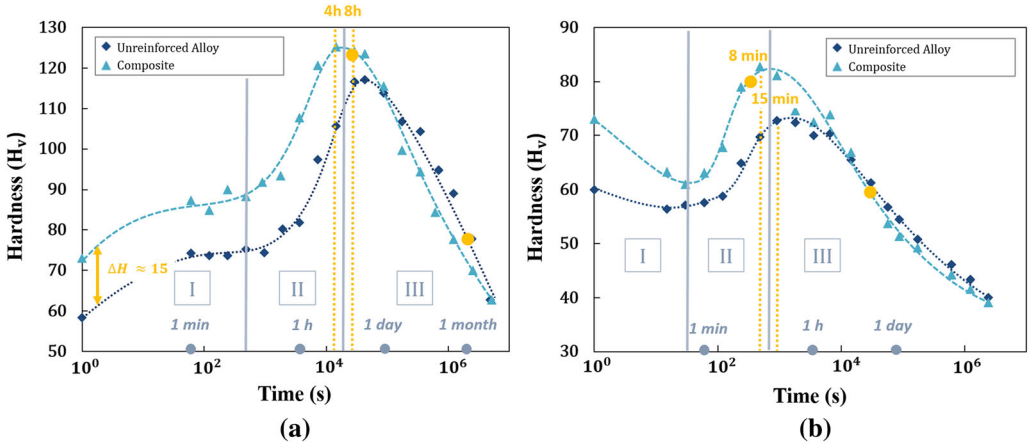

Fig. 2—Comparison of the hardness evolution of the unreinforced alloy and of the composite during isothermal aging at (*a*) 443 K (170 °C) and (*b*) 523 K (250 °C). The orange points correspond to the states which were chosen for the analysis by TEM (Color figure online).

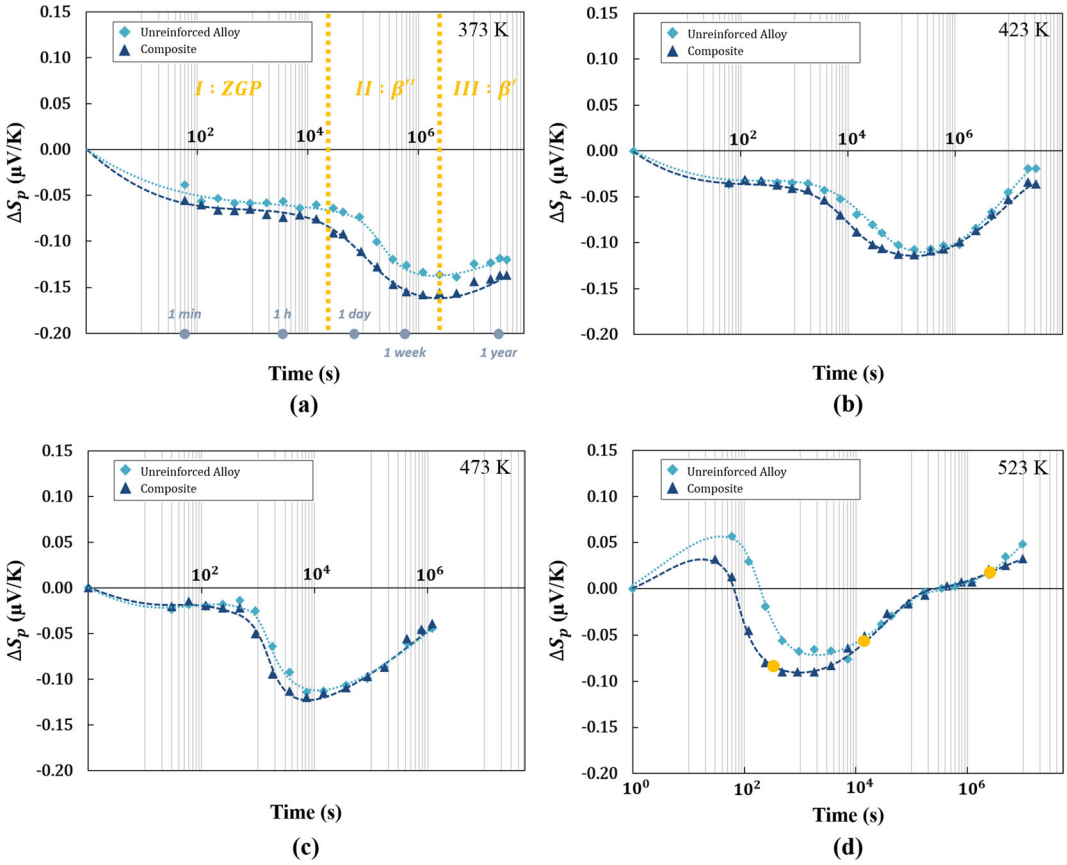

Fig. 3—Comparison of TEP kinetics at (*a*) 373 K (100 °C), (*b*) 423 K (150 °C), (*c*) 473 K (200 °C), and (*d*) 523 K (250 °C) of the alloy and of the composite. The orange points correspond to the states which were chosen for the analysis by TEM (Color figure online).

already reported in the literature for Al-Mg-Si alloys without silicon excess.

Lastly, beyond the hardness peak (domain III), further aging leads to the hardness drop corresponding to the precipitation of the semi-coherent phases.[1] The hardness decrease in this domain suggests that the semi-coherent precipitation began sooner and that there was an acceleration in the loss of strength beyond the hardness peak in the case of the reinforced alloy.

Figure 3 compares the precipitation kinetics of the unreinforced alloy and of the composite followed by measurements of the TEP variations (noted ΔS_p) between each aged state and the solution state during isothermal treatments at four temperatures between

373 K and 523 K (100 °C and 250 °C). These kinetics are likely to reflect the complex microstructural evolutions taking place in the alloy with or without ceramic particles and to highlight the difference in behavior between the alloy and its composite according to the aging temperature.

Just as with hardness variations, it is possible to distinguish three domains(I, II, III) on the TEP kinetics which are shown in Figure 3(a). Referring to the results of paper,[1] they correspond, respectively, to (i) the GP zone formation at $T < 523$ K (250 °C) or their dissolution at $T \geq 523$ K (250 °C)(domain I), (ii) the β'' precipitation (domain II), and (iii) the concomitant precipitation of semi-coherent phases (β'/Type-B for the unreinforced alloy) and of particles of pure silicon (domain III).

The TEP increase after the minimum of TEP kinetics can be partly explained by the fact that the semi-coherent phases are known to have a lower negative intrinsic effect on the TEP compared to β''. Consequently, the replacement of β'' by these phases is expected to contribute to the TEP increase. The strong TEP increase obtained in the present case can also be explained by the silicon precipitation in the form of coarse particles. Indeed, the departure of silicon from the solid solution may lead to a TEP increase.

In the temperature range studied, the TEP measurements clearly show that the kinetics of GP zone formation and the magnitude of the TEP variations due to this precipitation in domain I are very similar for the unreinforced alloy and reinforced alloy. This is consistent with the hardness results of Figure 2 and tends to support the fact that the ceramic particles have no strong influence on the GP zone formation in the present case. The TEP kinetics in domain II also confirm the acceleration of the coherent precipitation in the composite, as the beginning of the sharp TEP decrease due to this precipitation is shifted towards shorter aging times compared to the alloy's curves. Lastly, considering that the minimum of the TEP curves corresponds to the starting point for the transition between the coherent and semi-coherent precipitation, this phenomenon also seems to be accelerated in the case of the composite. Consequently, these observations are in rather good agreement with those obtained by hardness measurements.

2. *Non-isothermal precipitation curves of the reinforced and unreinforced alloy followed by DSC*

Figure 4 shows the DSC thermograms performed at a constant heating rate of 10 K/min for the alloy and the composite considered in this study. They confirm the tendencies highlighted by hardness and TEP measurements during isothermal aging. Firstly, an exothermic reaction due to the GP zone formation is observed at around 373 K (100 °C) for both materials confirming that GP zones precipitate even in the presence of ceramic particles in the matrix. Then, an endothermic peak at around 503 K (230 °C) reflects the dissolution of these zones. The peak temperature and magnitude are very similar for the two materials for both reactions, supporting the fact that the kinetics of GP zone

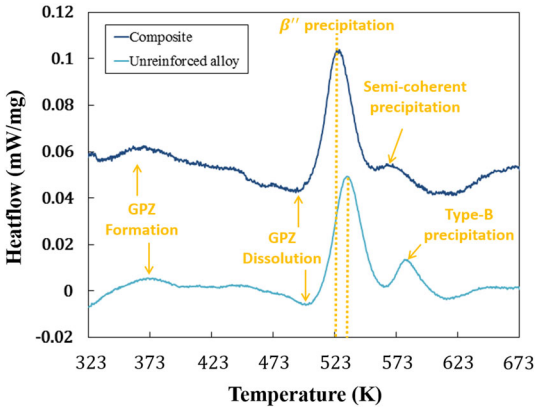

Fig. 4—Comparison between the alloy and composite DSC thermograms (scan rate 10 K/min) on solutionized and quenched samples (Color figure online).

formation and their volume fraction is comparable for both materials. This is consistent with previous studies of literature relative to a reinforced 6061 alloy[25] which suggested that the binding energy between the vacancies and the solute atoms (Mg, Si) is probably strong in Al-Mg-Si alloys. Hence, this could lead to the formation of solute–vacancy pairs which could be more prone to diffusing in the matrix to form clusters or GP zones, rather than being trapped by the sinks of the matrix.

A sharper peak corresponding to an exothermic reaction is detected at around 523 K (250 °C) and it can be unambiguously explained by the massive precipitation of the coherent β'' phase. As the peak due to this phase appears at a lower temperature in the composite, this indicates that this precipitation is accelerated in this material as was already highlighted in the preceding section by TEP and hardness. This has already been reported in the literature for 6061 alloys.

After this reaction, another exothermic reaction is detected at around 573 K (300 °C) with a lower amplitude. Based on the complete characterization of the alloy detailed in paper,[1] this sharp peak can be explained by the precipitation of the Type-B phase in the case of the alloy since it has been shown that this semi-coherent phase is the main phase after the precipitation of β'' during aging. In the case of the composite, the exothermic reaction probably corresponds to the semi-coherent precipitation. Compared to the peak of the alloy, one can note that the peak of the composite due to the semi-coherent precipitation is (i) broader, (ii) at a lower temperature, and (iii) not well dissociated from that due to the coherent precipitation suggesting a potential overlapping of phenomena in the composite material.

As a conclusion, most of the reactions described above lead to earlier apparition of peaks in the composite confirming the acceleration of kinetics when ceramic particles are added to the alloy.

After these preliminary studies, to understand which transformation is responsible for the behavior differences observed between the two materials, a TEM characterization of the metallurgical states for a more precise analysis was defined from the hardness and TEP

kinetics of Figures 2 and 3: (i) 8 hours and 1 month at 443 K (170 °C); (ii) 6 minutes, 8 hours and 1 month at 523 K (250 °C).

3. *Characterization of the microstructural evolutions during aging*

For C-TEM and HR-TEM characterization, the precipitates were observed along a $\langle 001 \rangle_{Al}$ direction. In these conditions, the precipitates appear as needles or rods. As their length is along a $\langle 100 \rangle_{Al}$ direction, three variants are visible on the micrographs: one variant is viewed end-on and the two others are viewed in projection in a {100} plane.

a. Comparison of the materials in peak-aged states The states obtained after 8 hours at 443 K (170 °C) (T6 state) and 6 minutes at 523 K (250 °C) were considered first because these treatments lead to microstructures responsible for the peak strength at each temperature (as can be seen in Figure 2). At 443 K (170 °C), the time of 8 hours was chosen (instead of 4 hours) as it leads to peak hardness values for the unreinforced and reinforced alloy. Indeed, the decrease in hardness of the composite material is only observed after 16 hours at 443 K (170 °C). At 523 K (250 °C), peak-aged conditions for the composite and slightly underaged conditions for the unreinforced alloy were noted after 6 minutes.

The microstructures of the alloy and of the composite, observed by C-TEM, after aging for 6 minutes at 523 K (250 °C) are shown in Figure 5. They provide evidence that the composite has a more heterogeneous microstructure than that of the alloy after the same thermal treatment. Indeed, in the reinforced alloy, two kinds of precipitation can be distinguished: a homogeneous precipitation uniformly distributed in the matrix (similar to the precipitation in the unreinforced alloy) and a heterogeneous precipitation of rods on dislocations. This observation supports the fact that a higher dislocation density is expected in the matrix of composite as proposed previously by different authors[17–19,31] and it tends to confirm that the dislocations act as preferential sites for heterogeneous nucleation.

HR-TEM investigations were carried out to analyze the nature of the precipitates in the alloy with or without ceramic particles. Figure 6 shows the different phases observed in the composite aged for 6 minutes at 523 K (250 °C) and Table II gives a summary of the phases detected in the two materials in the T6 state and in the state aged for 6 minutes at 523 K (250 °C).

While β'' was the only phase detected in the unreinforced alloy in these two states, various semi-coherent precipitates (Figures 6(c) through (f)) were observed in the matrix of the composite in addition to β'' (Figure 6(a)). Some of these phases nucleated homogeneously in the matrix such as the β'/β'_0, Type-B and Type-A phases. These phases probably formed during the early transformation of β''. By contrast, other precipitates were found to nucleate heterogeneously on the dislocations such as those shown in Figures 6(e) and (f). These precipitates growing on dislocations, named β'_{disloc} hereafter, demonstrated a disordered microstructure.

All these observations highlighted two main effects: (i) aging is accelerated in the matrix of the composite since several semi-coherent phases were detected in the matrix of the composite in the early stages of aging, (ii) dislocations are responsible for a heterogeneous precipitation which occurs in parallel with the homogeneous precipitation of β'. This latter point could explain the partial overlapping of the two exothermic peaks (due to β'' and to the semi-coherent precipitation) observed on the DSC curve in the case of the composite (Figure 4).

b. Comparison of the materials in over-aged states (1 month at 443 K (170 °C), 8 hours and 1 month at 523 K (250 °C)) For over-aged states, it was shown by HR-TEM that the β'' and semi-coherent phases detected in the composite in peak-aged conditions disappeared in favor of several types of semi-coherent precipitates such as the Type-B, Type-C and β' precipitates which were observed in the state aged for 8 hours at 523 K (250 °C) (Figure 7).

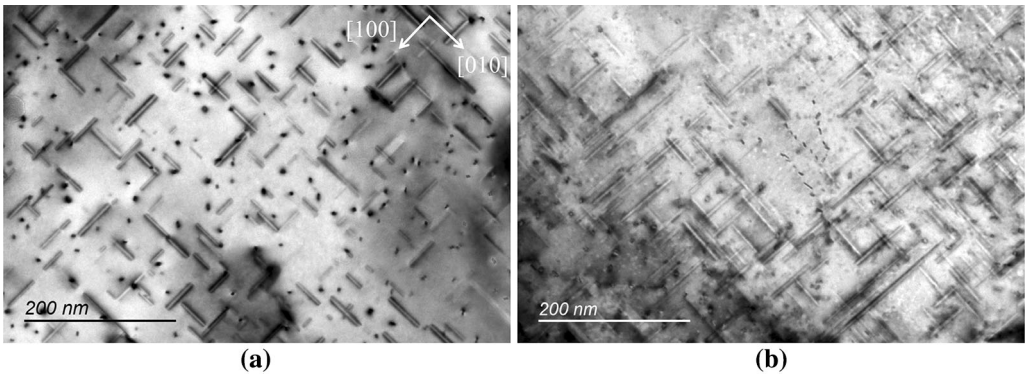

Fig. 5—Comparison of the C-TEM micrographs of (*a*) the unreinforced alloy and (*b*) the composite after being aged for 6 min at 523 K (250 °C) (zone axis : $\langle 001 \rangle_{Al}$).

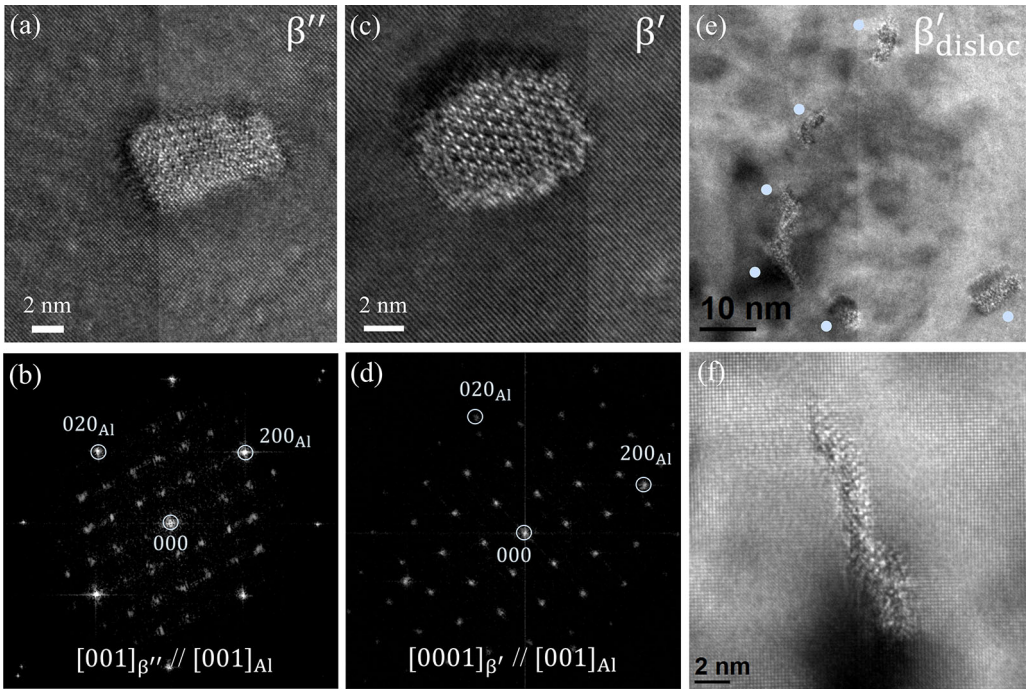

Fig. 6—HR-TEM images and corresponding FFT of (*a*, *b*) a β'' precipitate, (*c*, *d*) a β' precipitate, and (*e*, *f*) β'_{disloc} precipitates observed in the composite after being aged for 6 min at 523 K (250 °C) (zone axis : $\langle 001 \rangle_{Al}$).

Table II. Phases Observed in the Alloy and in the Composite in Peak-Aged Conditions at 443 K and 523 K (170 °C and 250 °C) with Their Mean Dimensions

			Phases	Mean Diameter (nm)	Mean Length (nm)
Peak conditions	T6 state (8 h at 443 K (170 °C))	alloy	**β''**	2 to 4	25 to 50
		composite	**β''**	2 to 5	—
			β'_0/Type-B	10 to 15	—
			Type-A	80	—
	6 min at 523 K (250 °C)	alloy	**β''**	3 to 5	40
		composite	**β''**	3 to 5	40
			β'_0/β'_{disloc}	10	40

The phases in the bold are the main phases identified in each state.

To analyze the microstructural evolutions occurring during the overaging of the alloy and of the composite more accurately, the main microstructural features of the states over-aged at 443 K and 523 K (170 °C and 250 °C) were summarized in Table III.

In the case of the unreinforced alloy, the main phase detected after peak aging is the phase of Type-B which tends to be gradually replaced by the phase of Type-C with further aging and later, by the Type-A phase.

In the case of the composite, the general tendency is the same as that of the unreinforced alloy but the precipitation sequence is notably accelerated. Indeed, the semi-coherent phases (β', Type-B), already detected in the peak-aged states at 443 K and 523 K (170 °C and 250 °C), were found to be rapidly replaced by the Type-C phase which becomes predominant in the states aged for 1 month at 443 K (170 °C) and 8 hours at 523 K (250 °C). This observation is consistent with previous studies of literature which have suggested that the Type-C precipitate prevails in the precipitation sequence of deformed excess Si alloys containing a high dislocation density, while the Type-B precipitate is hardly detected.[4] As a consequence, it seems that the dislocations present in the composite matrix promote the precipitation of the Type-C phase in over-aged states, by providing heterogeneous nucleation sites for the precipitation of this phase. In increasing the aging time at 523 K (250 °C) by up to 1 month, the Type-A precipitate predominates as in the case of the unreinforced alloy (Figure 8). Furthermore, due to the acceleration of the precipitation kinetics, the stable phase β-Mg_2Si has been observed in the composite after 1 month at 523 K (250 °C) while no sign of this phase has been observed in the unreinforced alloy.

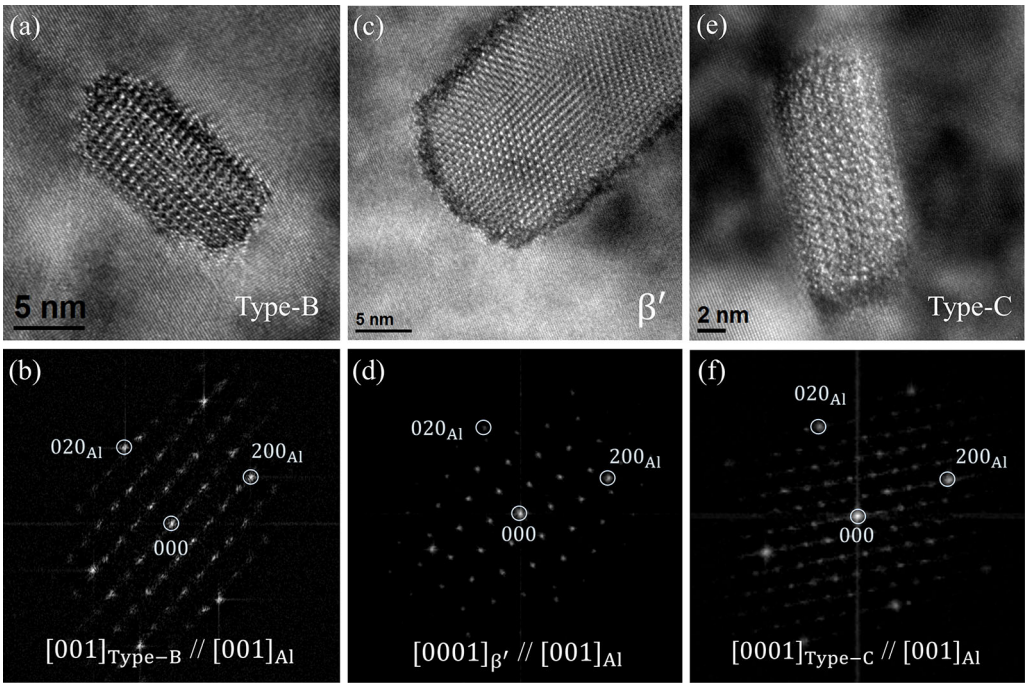

Fig. 7—HR-TEM images of the precipitates observed in the composite treated for 8 h at 523 K (250 °C): (*a*, *b*) a Type-B precipitate and its FFT, (*c*, *d*) the *β′* phase and its FFT, (*e*, *f*) the Type-C and its FFT (zone axis : $\langle 001 \rangle_{Al}$).

Table III. Summary of the Phases Observed in the Alloy and the Composite for Aging at 443 K and 523 K (170 °C and 250 °C) and the Corresponding Dimensions

			Phases	Mean Diameter (nm)	Mean Length (nm)
Over-aged conditions	1 month at 443 K (170°C)	alloy	*β″*	3 to 6	100 to 1000
			β′	6 to 10	100 to 1000
			type-B	6 to 15	100 to 1000
		composite	*β″*	10	1000 to 2000
			β'/β'_{disloc}	10 to 15	1000 to 2000
			type-B	10 to 15	1000 to 2000
			type-A	40 to 50	1000 to 2000
			type-C	8 to 50	1000 to 2000
	8 hours at 523 K (250°C)	alloy	*β′*	5 to 30	250 to 275
			type-A	30 to 80	250 to 275
			type-C	5 to 30	250 to 275
			type-B	5 to 30	250 to 275
		composite	*β′*	30 to 40	420
			type-C (type-A*)	10 to 30	420
	1 month at 523 K (250°C)	alloy	**type-A**	30 to 80	250 to 300
			type-B	5 to 30	250 to 300
			type-C	5 to 30	250 to 300
		composite	**type-A**	80 to 100	800
			type-C	5 to 30	800
			$\beta - Mg_2Si$	50 to 80	300 to 500

The phases in the bold are the main phases identified in each state (* corresponds to a precipitate non-observed but probably existing).

With regard to the precipitate dimensions (mean length and mean diameter) given in Table III, they are much higher in the composite, which is in line with the faster precipitation kinetics, due to the addition of ceramic particles in the alloy.

4. *Isothermal transformation curve*

Based on the coupling of the TEP kinetics performed between 373 K and 573 K (100 °C and 300 °C) with the microstructural observations detailed above, a part of the isothermal transformation curve of the studied composite maybe proposed and compared with the

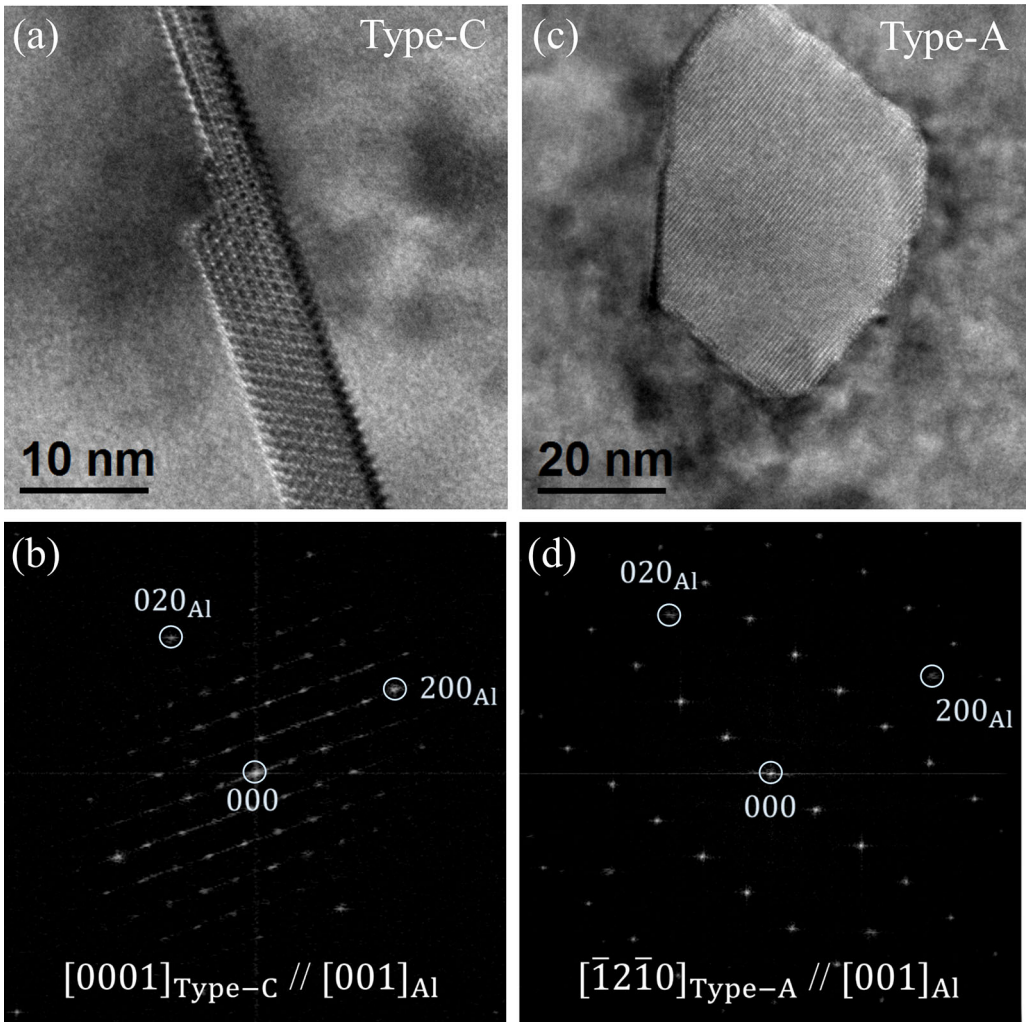

Fig. 8—Main precipitates observed after 1 month at 523 K (250 °C) in the composite: (*a*, *b*) Type-C phase and its FFT, (*c*, *d*) Type-A and FFT (zone axis : $\langle 001 \rangle_{Al}$).

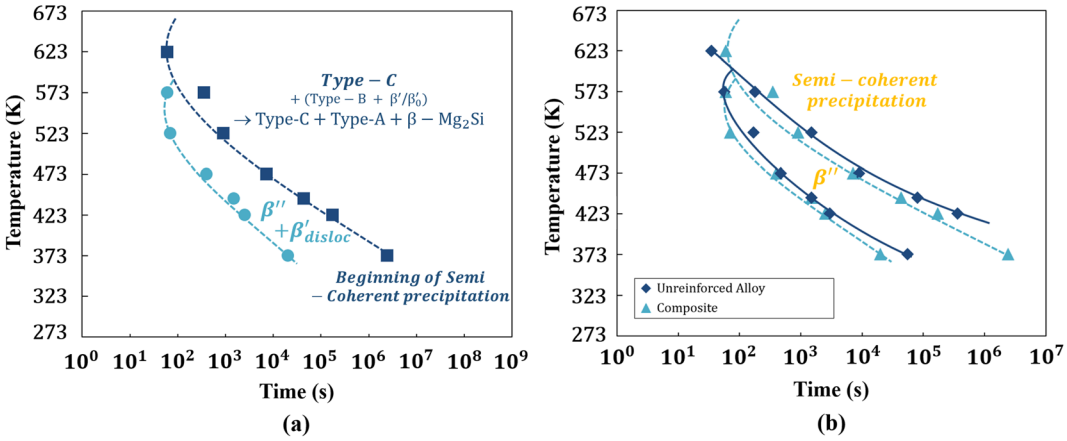

Fig. 9—(*a*) Part of the isothermal transformation curve obtained in this study for the composite; (*b*) comparison of the isothermal transformation curves of the alloy and the composite (Color figure online).

curve obtained for the alloy and presented in paper[1] (Figure 9). The same procedure as described in paper[1] was used. On the TEP kinetics shown in Figure 3, it was considered that:

– The time corresponding to the beginning of the β'' phase precipitation is defined by the intersection between the tangent to the decreasing part of the

curve due to β'' and the tangent to the part of the curve reflecting the GP zone formation,
- The time corresponding to the start of the precipitation of the semi-coherent phase is defined as the time corresponding to the minimum of the TEP kinetics.

Figure 9(a) illustrates that the coherent precipitation in the matrix of the composite is accompanied by the precipitation of a semi-coherent disordered phase, probably appearing during the early stages of aging on dislocations. Then, the β'' phase progressively disappears and the microstructure evolves in favor of the Type-C phase and later, of that of Type-A.

Figure 9(b) compares the isothermal transformation curves for the alloy and the composite. It reflects the acceleration of the precipitation kinetics of β'' in the composite and a decrease in the stability domain of this phase. The same tendency is highlighted for the semi-coherent precipitation which seems to begin sooner in the case of the composite.

B. *Analysis of the Effect of the Reinforcing Particles on the Decrease in Mechanical Strength During Aging from a T6 State*

Using the same procedure as that described in paper[1] for the unreinforced alloy, the T6-treated composite material of this study was isothermally aged at different aging temperatures between 373 K and 623 K (100 °C and 350 °C) and its hardness $H(t)$ was regularly measured (Figure 10(a)). Due to the thermal activation of the phenomena responsible for the hardness variations highlighted by the curves of Figure 10(a), a time–temperature equivalence based on an Arrhenius law with an activation energy Q was used to find the "equivalent time at 443 K (170 °C)" for all aging treatments performed at T and to build a unique master curve. Figure 10(b) shows that the superposition of the hardness curves is very good for an activation energy of 120 kJ/mol.

Taking into account the sigmoidal shape of the curves shown in Figure 10(a), the kinetics of Figure 10(a) were fitted by an isothermal Johnson–Mehl–Avrami–Kolmogorov (JMAK) model expressed by the following relation:

$$Y(T,t) = 1 - \exp(-(kt)^n), \qquad [3]$$

$$\text{with } k = k_0 \cdot \exp\left(-\frac{Q}{RT}\right), \qquad [4]$$

where $Y(T,t) = \frac{H(t)-H_{\max}}{H_{\min}-H_{\max}}$ is the transformed fraction ($0 < Y < 1$) with $H_{\min}$ the minimum hardness value and $H_{\max}$ the maximum hardness value (T6 state), n is the Avrami exponent (usually considered constant at different temperatures for a given transformation), k_0 is a

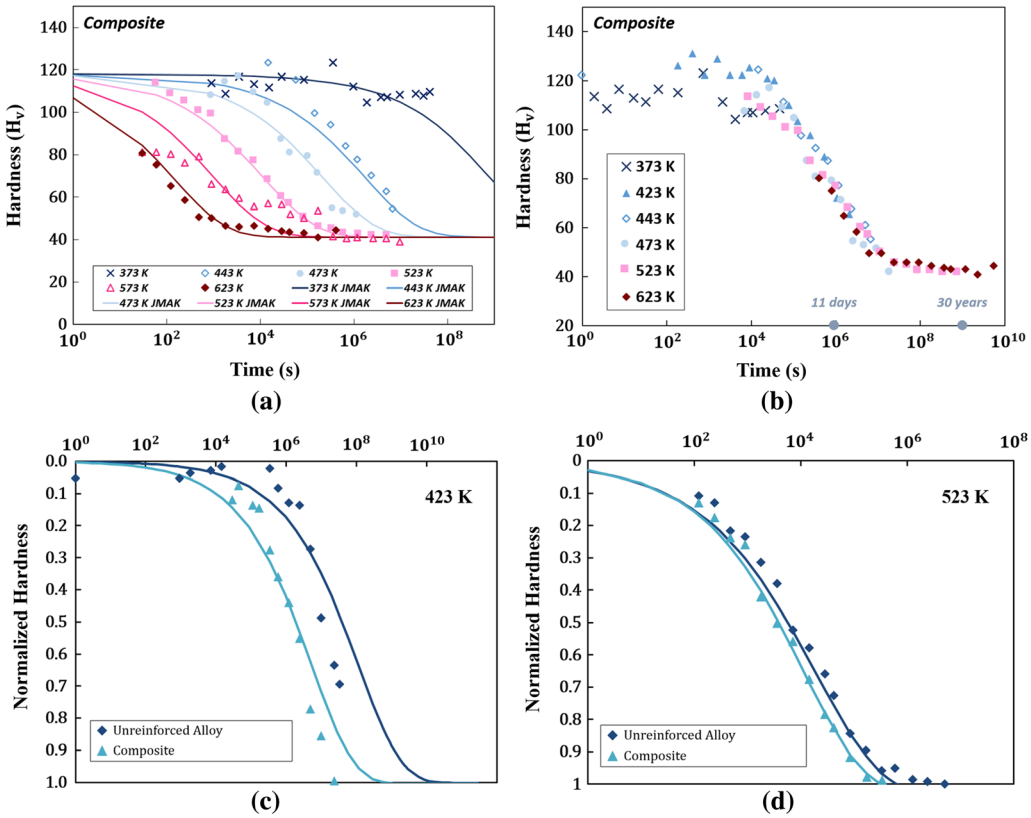

Fig. 10—(*a*) Hardness decrease measured from a T6 state and fitted with a JMAK law for different isothermal treatments between 373 K and 623 K (100 °C and 350 °C). (*b*) Time–temperature equivalence at 443 K (170 °C) for Q = 120 kJ/mol. Comparison of the normalized hardness evolution between the alloy and the composite for an aging at (*c*) 423 K (150 °C) and (*d*) 523 K (250 °C) (Color figure online).

constant, Q is the activation energy, T is the temperature, and R is the gas constant.

The JMAK model requires that three parameters, Q, n and k_0, be determined. Using the same method as that used in,[1] these parameters were determined for the composite and they were reported in Table IV where the parameters of the alloy (estimated in Reference 1) were also added for comparison. As can be seen in Figure 10(a), the hardness kinetics of the composite are well described with the parameters of Table IV.

To be able to compare the kinetics reflecting the loss of mechanical strength in the alloy and in the composite during aging from the T6 state, the curves giving the hardness variations, $\Delta H(t) = H(t) - H_{\max}$, of the two materials as a function of time were normalized by dividing $\Delta H(t)$ by $\Delta H_{\max} = H_{\min} - H_{\max}$.

The normalized hardness kinetics of both materials were plotted from the experimental data at 423 K and 523 K (150 °C and 250 °C) and they were also modeled with the JMAK model taking into account the parameters of Table IV, as can be seen in Figures 10(c) and (d). The curves shown in these figures clearly highlight the acceleration of the loss of mechanical strength in the reinforced alloy. Indeed, at both temperatures, the hardness decrease occurs earlier in the composite and due to this premature decrease in hardness, the minimum hardness value is also achieved earlier. This acceleration of the loss of mechanical properties can be explained by the acceleration of the precipitation kinetics due to the ceramic particles, leading to the presence of coarser semi-coherent phases likely to have a negative effect on the strength. However, it should be noted that the acceleration of the kinetics of the composite is more notable at the lowest aging temperature.

Taking into account the data in Table IV, it seems that the acceleration of the kinetics of strength loss in the composite is mainly due to the lower activation energy, Q, associated with the curves of this material. Indeed, the Avrami coefficients are not very different for both materials and the decrease in the k_0 value for the composite cannot explain an acceleration in kinetics.

It should be noted that a unique value was obtained for Q in the whole temperature domain in the case of the alloy and of the composite. This apparent activation energy can be compared with the activation energy for the diffusion of magnesium (130 kJ/mol) or that of silicon (124 kJ/mol) in aluminum.[54] For the alloy, as the measured activation energy (160 kJ/mol) is higher than that for the diffusion of Mg and Si, this suggests that the strength loss could be governed by two phenomena: the nucleation of the semi-coherent phases and the diffusion of the alloying elements. By contrast, for the composite, as the measured activation energy is very comparable to that for the diffusion of Mg and Si, this tends to indicate that the main phenomenon controlling the strength loss is the diffusion of these two elements which could be enhanced in the matrix of the composite due its high dislocation density. Indeed, dislocations are known to act as preferential diffusion paths likely to accelerate both the coherent and semi-coherent precipitation and the coarsening phenomena. Furthermore, they are likely to promote the nucleation of the semi-coherent phases as they provide heterogeneous nucleation sites.

IV. DISCUSSION

Combining different techniques (hardness, TEP, DSC), the present study has enabled us to provide evidence that the presence of ceramic particles in the investigated Al-Mg-Si alloy with a high silicon excess:

- has no strong influence on the kinetics of GP zone formation and on their quantity,
- accelerates the coherent precipitation of the β'' phase and the semi-coherent precipitation which is essentially due to the occurrence of the phase of Type-C after the hardness peak and later, to that of Type-A in the composite. Due to this acceleration, the peak strength of the reinforced alloy is reached earlier and the loss in mechanical strength occurs more rapidly than in the unreinforced alloy.

In the literature, many results of this type have already been reported in the case of Al-Mg-Si alloys without silicon excess.

For these alloys, the effect of the reinforcement on the kinetics of GP zone precipitation was not clearly identified since several conclusions (acceleration/retardation/suppression/absence of effect) were related. The present study is in favor of an absence of effect. As has already been reported in the literature,[25] this can be explained by fact that the quenched-in vacancies could form solute–vacancy pairs during quench due to a relatively high binding energy between Mg and Si and the vacancies. These pairs, which are supposed to be less mobile than free vacancies, could diffuse in the matrix to form GP zones instead of being trapped by the defects of the matrix (dislocations, interfaces). This is supported by the fact that a high concentration of vacancies has been already observed in the GP zones formed in the early stages of aging.[31,55–57]

Table IV. Summary of the JMAK Parameters for the Alloy (Cold-Rolled and Undeformed) and the Composite

	Alloy	Deformed Alloy (ε = 2.4 pct)	Composite
Q (kJ/mol)	160 (± 5)	135 (± 5)	120 (± 15)
n	0.35	0.34	0.38
$k_0(s^{-1})$	5.25×10^{11}	2.5×10^{9}	9.91×10^{7}

By contrast, the acceleration of the precipitation of the β'' and β' phases has been mentioned by several authors but it was not reported that a change in the type of semi-coherent precipitation sequence occurs. As recalled in the introduction of this paper, the explanations are based on an acceleration of the diffusion of the alloying elements due to the presence of residual stresses, interfaces and/or dislocations in the composite matrix. However, it is not very easy to identify which parameter prevails.

Knowing that the dislocations are generally considered to act as paths facilitating the solute atom diffusion in the matrix,[58] as preferential nucleation sites for semi-coherent phases[59] or as a trap for vacancies,[60] they are thus likely to have a strong effect on the mechanisms and kinetics of precipitation and to play a major role on the results presented in this study. This is why, the objective of the following discussion is to analyze precisely the contribution of the dislocations to the changes detected on the precipitation in the reinforced and unreinforced alloys.

The higher dislocation density in the composite matrix has already been well illustrated in the literature.[17–19] It is generally considered that the dislocation density is approximately ten times higher in the composite matrix than in the unreinforced alloy and this result is mainly explained by the great difference in the coefficient of thermal expansion (CTE) between the aluminum matrix and the ceramic particles. This parameter is known to be $25.5 \times 10^{-6}\ K^{-1}$ for aluminum and is of the order of $5 \times 10^{-6}\ K^{-1}$ in the case of ceramic particles.[61–64] Hence the considerable difference in CTE results, during cooling from a high temperature, in a higher dislocation density near the particles due to the plastic accommodation of the deformation incompatibility.

A. *Dislocation Density in the Composite Matrix Determined by ECCI*

The dislocation density of the composite matrix has been estimated in this study by ECCI to confirm that ceramic particles lead to a high dislocation density.

The dislocation density was estimated in two different grains located near to or far from a carbide particle (Figures 11(a) through (c)) and it was plotted as a function of the distance from the particle interface (Figure 11(d)). A density of $9.3 \times 10^{13}\ m^{-2}$ was measured at 3 μm from the interface, while a density of $4.5 \times 10^{13}\ m^{-2}$ was found at 30 μm from the interface. This leads to a mean dislocation density of the order of $7.0 \times 10^{13}\ m^{-2}$. This value is comparable to the dislocation densities, determined experimentally by TEM, by different authors,[31,65] since dislocation densities reaching $10^{14}\ m^{-2}$ have been reported. By contrast, it is much higher than the dislocation density calculated using the Arsenault and Shi model[65] in the case of an aluminum matrix composite reinforced with equiaxed particles. In

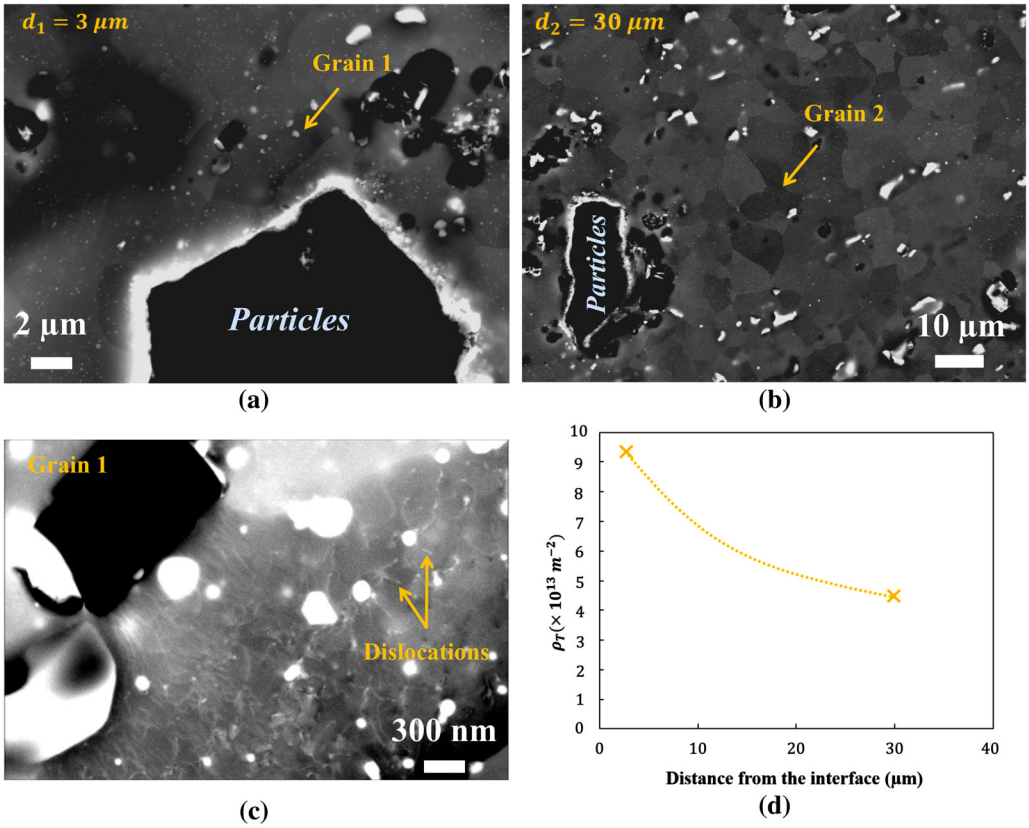

Fig. 11—Estimation of dislocation density using ECCI technique in 2 different grains: (*a*, *c*) a grain near the particle interface and (*b*) a grain in the matrix. (*d*) Plot of the dislocation density as a function of the distance from the particle interface (Color figure online).

this case, the estimated dislocation density is of the order of 3×10^{12} m^{-2}.

The increase in yield strength ($\Delta\sigma_y$) due to the dislocations created in the composite matrix during cooling from high temperature can be expressed by the following relation:

$$\Delta\sigma_y = \alpha M \mu b \sqrt{\rho}, \quad [5]$$

where α is a constant comprised between 0 and 1 (estimated as being equal to 0.27 by Deschamps *et al.*[66]), M is the Taylor factor considered to be between 2 and 4,[67] μ is the shear modulus of aluminum (2.86×10^4 MPa) and b is the Burgers vector (2.86×10^{-10} m).[68,69] Taking into account the data reported in the literature, the value of the product αM can be estimated as being comprised between 0.5 and 1.

Using this data and taking into consideration the mean dislocation density measured in the composite matrix, the increase in yield strength ($\Delta\sigma_y$) due to the dislocations can be estimated between 34 and 68 MPa. Assuming that the increase in yield strength ($\Delta\sigma_y$) is related to the increase in hardness (ΔH) according to the following relation: $\Delta\sigma_y \approx 3 \times \Delta$H, one can estimate that the increase in hardness due to the dislocations should be between 11 and 22. This result is consistent with the data in Figure 2 which leads to a value of ΔH of 15 in the as-quenched state of the composite.

As a conclusion to this section, the distribution of the dislocations within the composite was not found to be uniform, since a higher dislocation density was detected near the interface. This thus confirms that ceramic particles generate an increase in the dislocation density in the matrix compared with the unreinforced alloy during cooling from the solutionizing temperature. In this context, the next sections will focus on the effect of the introduction of dislocations in an unreinforced alloy on the mechanisms and kinetics of precipitation.

B. *Effect of the Dislocations on Precipitation Kinetics During Aging from the Solid Solution State*

To determine experimentally the effect of the presence of a high dislocation density in the studied alloy, the unreinforced alloy was cold-rolled with two different reduction ratios (1.5 and 2.4 pct) after homogenization at 813 K (540 °C) and water-quench. The samples of the deformed alloy were then artificially aged at 443 K (170 °C) and their hardness and TEP were measured during aging.

Figure 12(a) shows how the hardness evolves during the aging treatment at 443 K (170 °C) in deformed alloys compared with the undeformed alloy and the composite.

The first striking observation is that the hardness kinetics of the deformed alloys and that of the composite are perfectly superimposed and differ notably from that of the undeformed alloy. In the initial state (after a solutionizing treatment), one can note that the hardness values of the deformed alloys and of the composite are similar, confirming that the higher initial hardness value of the composite compared to that of the unreinforced alloy is mainly due to the dislocations generated in the matrix of the composite due to the CTE mismatch between the matrix and particles. In other words, this means that the contribution of the ceramic particles to the hardness (due to back stress as a result of particles resisting the plastic flow of the matrix) is probably lower than the strengthening due to the CTE mismatch. Then, the hardness increase linked to the precipitation of β'' occurs simultaneously in the deformed alloys and the composite and leads to the same peak hardness value being achieved at the same time (4 hours). Lastly, the loss of strength follows the same slope and is detected earlier than in the undeformed alloy.

The same tendencies can be deduced from the TEP variations shown in Figure 12(b). Indeed, the main TEP decrease, attributed to the β'' precipitation, starts for shorter aging times when the alloy was deformed before aging or is reinforced with particles and the minimum TEP value corresponding to the starting point of the semi-coherent precipitation is reached earlier for the composite and the deformed alloys.

Another important point is that increasing the dislocation density with an increase in the reduction ratio was not found to have a strong effect on the kinetics of hardness and TEP evolution, suggesting that a limit deformation above which no further evolution can be detected on the precipitation kinetics, exists.

In conclusion, these investigations on deformed alloys showed that the differences detected on the precipitation kinetics of the alloy and of the composite can be justified by the presence of a high dislocation density in the matrix of the composite. The dislocations are likely to accelerate the coherent precipitation of β'' due to an enhanced diffusion of Mg and Si. In addition, they promote the semi-coherent precipitation which is detected for shorter aging times.

C. *Effect of the Dislocations on the Precipitation Sequence*

After having shown the influence of the dislocations on the precipitation kinetics, HR-TEM observations were performed on the cold-rolled alloy to check if the addition of dislocations is responsible for the microstructural differences observed previously between the alloy and the composite. For this study, the undeformed alloy was cold-rolled, after homogenization, with a reduction ratio of 2.4 pct and it was aged for 8 hours at 523 K (250 °C) before HR-TEM characterization. Three types of precipitates were detected: the β'' phase and the phases of Type-B and Type-C. As in the case of the composite treated in the same conditions, the predominant phase is that of Type-C, illustrated in Figure 13, while the main phase detected in the unreinforced alloy is that of Type-B. Hence, these observations confirm that dislocations promote the precipitation of the Type-C phase, which is in good agreement with a previous study suggesting that this phase preferentially precipitates on dislocations.[4]

From the HR-TEM study on the deformed alloy and on the composite, it may be concluded that dislocations are likely to change the semi-coherent precipitation both

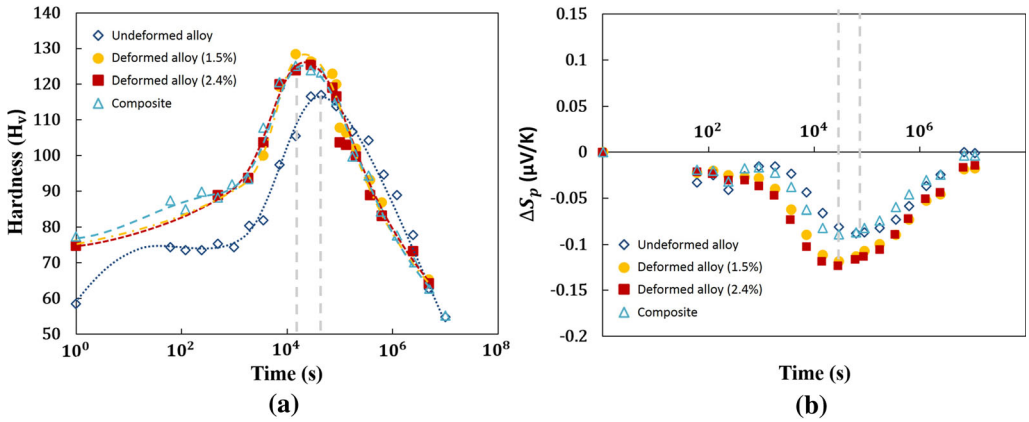

Fig. 12—Comparison of the (*a*) hardness kinetics and (*b*) TEP kinetics during aging at 443 K (170 °C) for the unreinforced alloy, deformed alloys and the composite (Color figure online).

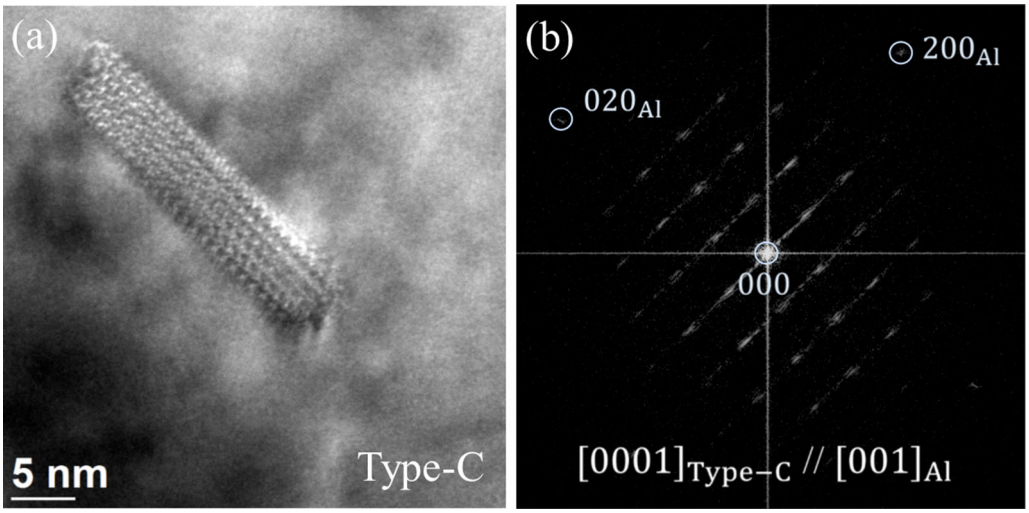

Fig. 13—HR-TEM image of (*a*) the Type-C precipitate, main phase observed in the cold-rolled alloy (with a deformation ratio of 2.4 pct) after aging for 8 h at 523 K (250 °C) and (*b*) its FFT (zone axis : $\langle 001 \rangle_{Al}$).

in peak-aged and over-aged states. In the peak-aged states of the composite, it became apparent that the dislocations tend to promote the precipitation of disordered phases (Figures 6(e) and (f)), which is consistent with previous studies on pre-deformed alloys.[66,67] In over-aged states, the dislocations were found to modify the relative proportion of the semi-coherent phases (β', Type-A, Type-B, Type-C) compared to that of the unreinforced alloy. This is also in agreement with results of literature showing that dislocations promote phases less observed in undeformed alloys[70,71] and even the Type-C phase.[72]

D. *Analysis of the Decrease in Mechanical Strength of the Alloy During Aging from a T6 State*

To evaluate the effect of the presence of a high density of dislocations on the decrease in hardness of the alloy during aging from a T6 state, the unreinforced alloy was deformed by cold-rolling with a reduction ratio of 2.4 pct, T6-treated and then aged at different temperatures between 443 K and 623 K (170 °C and 350 °C). The same procedure as that used for the unreinforced alloy and for the composite in Section III–B was used to determine the parameters of the JMAK law of the deformed alloy: $Q = 135$ kJ/mol, $n = 0.34$, $k_0 = 2.5 \times 10^9$ s^{-1}. Comparing these parameters to those of the alloy and of the composite (given in Table IV), it can be noted that the effect of the high dislocation density in the alloy is to decrease the values of Q and k_0, which tend to approach those of the composite material. These results thus confirm the fact that the dislocations play a major role in the acceleration of the loss of strength of the composite material as they are likely to promote the diffusion of the solute elements in the matrix of the composite and the nucleation of the semi-coherent phases.

The consequences of these results are summarized in Figure 14 where the hardness decrease predicted by the JMAK law for the alloy, the deformed alloy and the

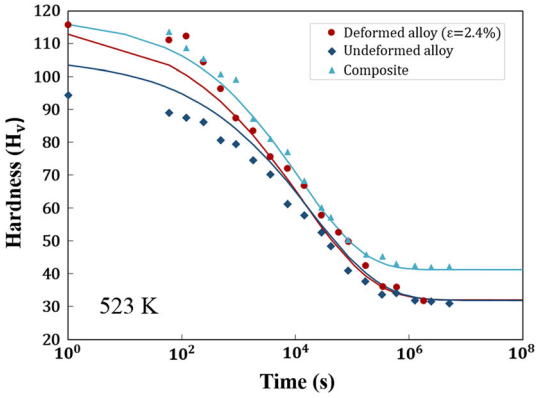

Fig. 14—Comparison of the decrease in hardness from the T6 state during aging at 523 K (250 °C) predicted by the JMAK law for the undeformed alloy, the cold-rolled alloy and the composite (Color figure online).

composite are compared for an aging at 523 K (250 °C). At this relatively high temperature, it can be pointed out that the curves of the deformed alloy and of the composite are very similar in the early stages of the treatment and present a slight acceleration compared to the curve of the alloy. However, for the longer aging times, the curve of the deformed alloy tends to approach that of the unreinforced alloy and to reach the same final value (Hv_{min} = 32). Since the alloy and the deformed alloy reach the same final hardness value while their initial value was different due to strain hardening, this suggests that the recovery and recrystallization phenomena probably took place in the deformed alloy for the long aging times at 523 K (250 °C) leading to a slowdown of the kinetics of the deformed material. As these phenomena probably also occurred in the composite and due to the slight acceleration of the kinetics of this material at all aging times (as can be seen in Figures 10(c) and (d)), one can suggest that other factors facilitating the diffusion of the elements in solid solution such as the interfaces or grain boundaries could exist in the composite and may contribute to the acceleration of the kinetics. However, these factors are not expected to be predominant compared to the effect of the high dislocation density (which is particularly visible at low temperature (≈ 423 K (150 °C)) where the recovery phenomena are supposed to be notably delayed and less marked).

V. CONCLUSION

The present study has enabled us to show the following points relative to the effect of the presence of ceramic particles in an Al-Mg-Si alloy with a high silicon excess during aging between 373 K (100 °C) and 623 K (350 °C):

1. From a microstructural point of view, it was clearly highlighted that the ceramic particles do not affect the kinetics of GP zone formation and their density. By contrast, they lead to an acceleration in the coherent and semi-coherent precipitation, which leads to an acceleration in the kinetics of strength loss of the composite material from a T6 state compared to that of the unreinforced alloy.
2. The TEM characterization proved that the presence of reinforcement also induces microstructural modifications during aging. First, in peak-aged states, it was shown that the microstructure of the composite is more heterogeneous than that of the alloy since it combines both coherent and semi-coherent phases. Some of these semi-coherent precipitates which nucleated on dislocations during the earliest stage of composite aging were found to have a disordered structure. In over-aged states, it was observed that the Type-C phase was mainly responsible for the composite's loss of strength, while it is that of Type-B in the unreinforced alloy. Nevertheless, for prolonged overaging, the Type-A phase was found to prevail in both cases.
3. The unreinforced alloy was deformed to analyze more precisely the role of the increased dislocation density in the composite matrix. This led us to show that dislocations are mainly responsible for the acceleration of the aging and overaging kinetics in the case of the composite (notably, at low temperature ($T \leq 473$ K (200 °C))) and for the microstructural differences observed during aging between the alloy and the composite.
4. The comparison between the isothermal transformation curves of the alloy and of the composite showed that the stability domains of the coherent and semi-coherent precipitation are lowered in the composite, as the higher dislocation density in the composite matrix promotes the nucleation of semi-coherent phases.
5. The prediction of the hardness evolution during isothermal aging from a T6 state was performed in this study using a JMAK approach to be able to compare the mechanical behavior of the alloy and of the composite for long aging times. This approach highlighted that the reinforcing particles accelerate the loss of strength, especially at the low staging temperatures of the investigated temperature domain. This was mainly attributed to the decrease in the activation energy (Q) of hardness drop for composite, due to the high dislocation density in the composite matrix, which promotes the diffusion of the alloying elements in the composite matrix and the nucleation of the semi-coherent phases. The use of the same JMAK approach for the deformed alloy led us to the conclusion that the high dislocation density in the matrix of the unreinforced alloy also decreases the activation energy (Q) of the JMAK law. It was thus suggested that the dislocations are the main factor responsible for the acceleration of the loss in composite strength as long as the recovery phenomena do not come into play.

ACKNOWLEDGMENTS

We would like to thank the Clym (Consortium Lyonnais de Microscopie) for access to the 2010F and 2100 microscope and to N. Blanchard for his kind assistance with the Conventional TEM observations. The authors are also grateful to Dr. S.Cazottes for her support with the ECCI technique.

REFERENCES

1. G. Meyruey, V. Massardier, W. Lefebvre, and M. Perez: *Mater. Sci. Eng. A*, 2018, vol. 730, pp. 92–105.
2. K. Fukui, M. Takeda, and T. Endo: *J. Jpn. Inst. Met.*, 2006, vol. 70, pp. 715–19.
3. A.K. Gupta, D.J. Lloyd, and S.A. Court: *Mater. Sci. Eng.*, 2001, vol. 316, pp. 11–17.
4. K. Matsuda, Y. Sakaguchi, Y. Miyata, Y. Uetani, T. Sato, A. Kamio, and S. Ikeno: *Mater. Sci.*, 2000, vol. 5, pp. 179–89.
5. K. Matsuda, S. Tada, S. Ikeno, T. Sato, and A. Kamio: *Scripta Metall. Mater.*, 1995, vol. 32, pp. 1175–80.
6. K. Matsuda, S. Ikeno, T. Sato, and A. Kamio: *Acta Metall.*, 1996, vol. 34, pp. 1797–1802.
7. K. Matsuda, T. Naoi, K. Fujii, and Y. Uetani: *Mater. Sci. Eng. A*, 1999, vol. 262, pp. 232–37.
8. A. Froseth, S. Andersen, C. Marioara, P. Derlet, and R. Hoier: *MRS Online Proceeding Libr. Arch.*, 2002.
9. A. Froseth, R. Hoier, P. Derlet, S. Andersen, and C. Marioara: *Phys. Rev. B*, 2003, vol. 67, pp. 1–11.
10. L.C. Doan, K. Nakai, Y. Matsuura, S. Kobayashi, and Y. Ohmori: *Mater. Trans.*, 2002, vol. 43, pp. 1371–80.
11. C. Ravi and C. Wolverton: *Acta Mater.*, 2004, vol. 52, pp. 4213–27.
12. E. Povoden-karadeniz, P. Lang, P. Warczok, A. Falahati, W. Jun, and E. Kozeschnik: *Calphad*, 2013, vol. 43, pp. 94–104.
13. S. Mazumdar: *Composites Manufacturing*, 2016, pp. 1–6.
14. Lucintel: Report, Growth opportunities in Global Composites Industry,Lucintel, Texas (USA), pp. 1-25, March 2011.
15. L. Berreur, B. DeMaillard, and S. Nosperger: *Report, Nodal Consultants*, Paris, pp. 1-30, May 2002.
16. F. Humphreys, H. Lilholt, and O. Pederson:*Proc. 9th Riso Int. Symp. Mech. Phys. Behav. Met. Ceram. Compos.*, 1988, pp. 51–74.
17. S. Suresh and T. Christman: *Scripta Metall.*, 1989, vol. 23, pp. 1599–1602.
18. R.J. Arsenault, L. Wang, and C.R. Feng: *Acta Metall. Mater.*, 1991, vol. 39, pp. 47–57.
19. M. Vogelsang, R.J. Arsenault, and R.M. Fisher: *Metall. Trans. A*, 1986, vol. 17, pp. 379–89.
20. Z.M. Sun, J.B. Li, Z.G. Wang, and W.J. Li: *Acta Met. Mater.*, 1992, vol. 40, pp. 2961–66.
21. M. Suery, C. Teodosiu, and L.F. Menezes: *Mater. Sci. Eng.*, 1993, vol. 167, pp. 97–105.
22. N.K. Sharma, R.K. Misra, and S. Sharma: *Ceram. Int.*, 2017, vol. 43, pp. 513–22.
23. N. Ramakrishnan: *Acta Mater.*, 1996, vol. 44, pp. 69–77.
24. G. Meijer, F. Ellyin, and Z. Xia: *Compos. Part B Eng.*, 2000, vol. 31, pp. 29–37.
25. V. Massardier and P. Merle: *Mater. Sci. Eng. A*, 1998, vol. 249, pp. 109–20.
26. D. Dafir, G. Guichon, R. Borrelly, S. Cardinal, P.F. Gobin, and P. Merle: *Mater. Sci. Eng. A*, 1991, vol. 144, pp. 311–18.
27. P. Appendino, C. Badini, F. Marino, and A. Tomasi: *Mater. Sci. Eng.*, 1991, vol. 135, pp. 275–79.
28. C. Badini, F. Marino, and A. Tomasi: *Mater. Sci. Eng.*, 1991, vol. 136, pp. 99–107.
29. N.E. Bekheet, R.M. Gadelrab, M.F. Salah, and A.N.A. El-azim: *Mater. Des.*, 2002, vol. 23, pp. 153–59.
30. J.M. Papazian: *Metall. Trans. A*, 1988, vol. 19 (12), pp. 2945–53.
31. I. Dutta, S.M. Allen, and J.L. Hafley: *Metall. Trans. A*, 1991, vol. 22, pp. 2553–63.
32. S. Abis and G. Donzelli: *J. Mater. Sci. Lett.*, 1988, vol. 7, pp. 51–52.
33. C. Friend and S. Luxton: *J. Mater. Sci.*, 1988, vol. 23, pp. 3173–80.
34. T.G. Nieh and R.F. Karlak: *Scripta Metall.*, 1984, vol. 18, pp. 25–28.
35. M. Hadianfard, Y. Mai, and J. Healy: *J. Mater.*, 1993, vol. 28, pp. 3665–69.
36. M. Gupta and M. Surappa: *Mater. Res. Bull.*, 1995, vol. 30, pp. 1023–30.
37. L. Salvo, G. L'Esperance, M. Suery, and J. Legoux: *Mater. Sci. Eng.*, 1994, vol. 177, pp. 173–83.
38. C. Badini, F. Marino, and A. Tomasi: *Mater. Chem. Phys.*, 1990, vol. 25, pp. 57–70.
39. S. Reihani, D. Dafir, and P. Merle: *Scripta Metall. Mater.*, 1993, vol. 28, pp. 639–44.
40. D. Dafir: Ph.D. Thesis, INSA de Lyon, 1993.
41. L. Nordheim and C.J. Gorter: *Physica*, 1935, vol. 2, pp. 383–90.
42. J. Blatt and F.J. Lucke: *Philos. Mag.*, 1967, vol. 15, pp. 649–57.
43. J.E. Hatch: *Aluminium: Properties and Physical Metallurgy*. American Society for Metals, ASM International, 1984.
44. G.M. Raynaud and P. Guyot: *Acta Metall.*, 1988, vol. 36, pp. 143–47.
45. J.M. Pelletier, G. Vigier, J. Merlin, P. Merle, F. Fouquet, and R. Borrelly: *Acta Metall.*, 1984, vol. 32, pp. 1069–78.
46. J.M. Pelletier: Ph.D. Thesis, INSA de Lyon, 1980.
47. J. Ahmed, A.J. Wilkinson, and S.G. Roberts: *Philos. Mag. Lett.*, 1997, vol. 76, pp. 237–45.
48. M.A. Crimp: *Micros. Res. Tech.*, 2006, vol. 69, pp. 374–81.
49. A.J. Wilkinson and P.B. Hirsch: *Micron*, 1997, vol. 28, pp. 279–308.
50. D. M. Norfleet, D. M. Dimiduk, S. J. Polasik, M. D. Uchic, and M. J. Mills: *Acta Mater.*, 2008, pp. 2-14.
51. U. Martin, U. Muhle, and H. Oettel: *Prakt. Metallogr.*, 1995, vol. 32, p. 467.
52. H. Demers, N. Poirier-Demers, A. Real Couture, D. Joly, M. Guilmain, N. De Jonge, D. Drouin (2011) *Scanning*, vol. 33, pp. 135–46.
53. S. Zaefferer and N.N. Elhami: *Acta Mater.*, 2014, vol. 75, pp. 20–50.
54. H. Hunsicker: *Aluminium* (vol. 1), *ASM*, Metal. Ohio, 1967.
55. V. Fallah, B. Langelier, N. Ofori-opoku, and B. Raeisinia: *Acta Mater.*, 2016, vol. 103, pp. 290–300.
56. A. Lutts: *Acta Metall.*, 1961, vol. 9, pp. 577–86.
57. S.J. Andersen, H.W. Zandbergen, J. Jansen, C. TrÆholt, U. Tundal, and O. Reiso: *Acta Mater.*, 1997, vol. 46, pp. 3283–98.
58. J. Hoyt: *Acta Metall.*, 1972, vol. 39, pp. 2091–98.
59. FC Larché: *Dislocations in Solids*, North-Holland, Amsterdam, 1979, vol. 4, p. 135.
60. M. Wintenbergers: *Acta Metall.*, 1959, vol. 7, pp. 549–55.
61. HJ Rack: *Adv. Mater. Manuf. Process.*, 1988, vol. 3, pp. 327–58.
62. J.F. Lynch, C.G. Ruderer, and W.H. Duckworth: *Engineering Properties of Selected Ceramic Materials*, Batelle Memorial Institute, The American Ceramic Society, Columbus, 1966.
63. A Geiger and M Jackson: *Adv. Mater. Process.*, 1989, vol. 7, p. 23.
64. W Lengauer: *Handbook of Ceramic Hard Materials (Transition metal carbides, nitrides and carbonitrides)*, Wiley, New-York, 2003, pp. 202–03.
65. R.J. Arsenault and N. Shi: *Mater. Sci. Eng.*, 1986, vol. 81, pp. 175–87.
66. A. Deschamps, F. Livet, and Y. Bréchet: *Acta Mater.*, 1999, vol. 47, pp. 281–92.
67. M.J. Starink and S.C. Wang: *Acta Mater.*, 2003, vol. 51, pp. 5131–50.
68. F. Humphreys: *Acta Met. mater.*, 1977, vol. 25, pp. 1323–44.
69. N. Hansen: *Acta Met. Mater.*, 1977, vol. 25, pp. 863–69.
70. K. Teichmann, C.D. Marioara, S.J. Andersen, K.O. Pedersen, S. Gulbrandsen-Dahl, M. Kolar, R. Holmestad, and K. Marthinsen: *Philos. Mag.*, 2011, vol. 91, pp. 3744–54.
71. R.S. Yassar, D.P. Field, and H. Weiland: *Scripta Mater.*, 2005, vol. 53, pp. 299–303.
72. K Matsuda, S Shimizu, H Gamada, Y Uetani, F Shinagawa, and S Ikeno: *J. Soc. Mat. Sci.*, 1999, vol. 48, pp. 10–15.